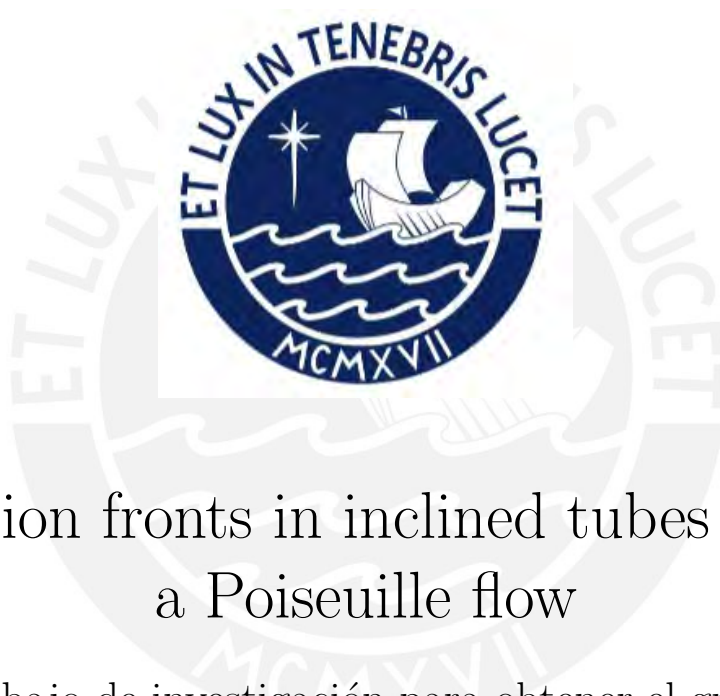# Pontifica Universidad Católica del Perú

Escuela de Posgrado

Reaction fronts in inclined tubes under a Poiseuille flow

Trabajo de investigación para obtener el grado
académico de Magíster en Física que presenta:

Rodrigo Miguel Rivadeneira Vizcardo

Asesor:
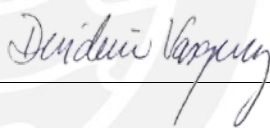**Desiderio Augusto Vásquez Rodríguez**

Lima, 2022

Declaración jurada de autenticidad

Yo, Desiderio Augusto Vásquez Rodríguez, docente de la Escuela de Posgrado de la Pontificia Universidad Católica del Perú, asesor de la tesis titulada *Reaction fonts in inclined tubes under a Poiseuille Flow* del autor Rodrigo Rivadeneira Vizcardo, dejo constancia de lo siguiente:

- El mencionado documento tiene un índice de puntuación de similitud de 17%, lo que está dentro del límite establecido. Así lo consigna el reporte de similitud emitido por el software *Turnitin* el 24/08/2022.
- He revisado con detalle dicho reporte y confirmo que cada una de las coincidencias detectadas no constituyen plagio alguno.
- Las citas a otros autores y sus respectivas referencias cumplen con las pautas académicas.

Lima,   29 de noviembre de 2022

Apellidos y nombres del asesor: Vásquez Rodríguez, Desiderio Augusto	
DNI: 06480334	Firma:
ORCID: 0000-0003-2436-7221	

Dedication

Teachers play an indispensable role in the formation of researchers and professionals. As a researcher, I have been formed by my teachers' leadership and example. As an educator I have been given the chance to see experts at work everyday. I would not have been able to complete this work without the motivation and encouragement from my teachers. I hope that I may do for my students what they have done for me. For this reason, this work is dedicated to all my teachers, past, present and future.
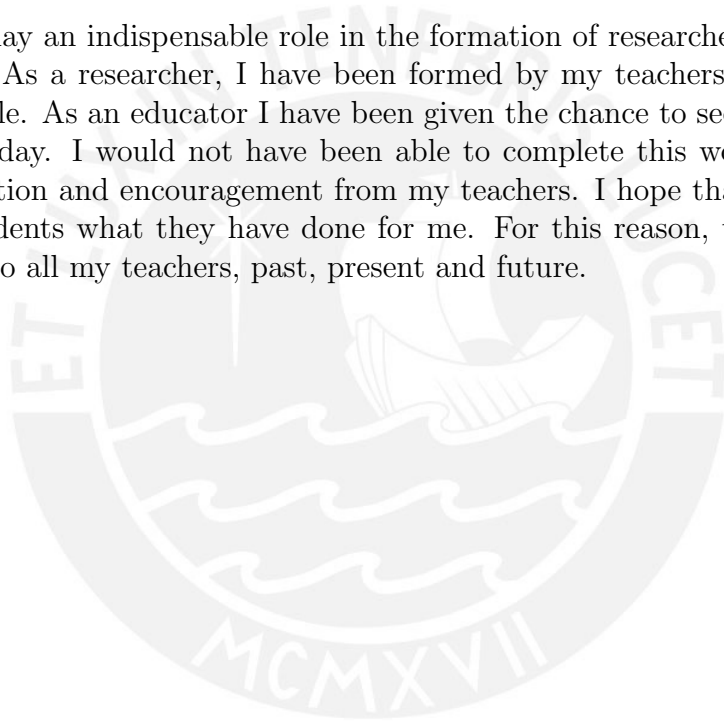
Acknowledgements

This work would not have been possible without the support of key people and institutions within the Pontificia Universidad Católica del Perú (PUCP).

Firstly, I would like to express my gratitude to the PUCP. Through the Programa de Apoyo a la Iniciación en la Investigacion (PAIN) the University recognised the work here presented as a promising study in 2008. Through the presentation of this thesis I would like to show, in return, my recognition to their support in my beginnings as a researcher.

Secondly, I would like to acknowledge the unconditional and selfless support provided by the Physics Department at PUCP. Both, administrative staff and teachers have always demonstrated admirable support and a willingness to empower my research capabilities. For as long as this thesis took to be produced, the people in the Department have provided advise, guidance and help towards assuring that the project is completed. In particular, I would like to thank the support given by Prof. Maria Elena López, who served as coordinator of the Master's program since before I started this work until last year. Her assistance went beyond what was expected of a coordinator demonstrating exemplary encouragement always.

Finally and most importantly, I must express my deepest and most sincere gratitude to Prof. Desiderio Vasquez, who served as my advisor through the entirety of this thesis. The work presented is based on his previous studies and accomplishments. I am indebted to Prof. Vasquez for sharing his work and insights so openly. Since the start of the project through to the end, Prof. Vasquez shared otherwise unobtainable insights into his published work. His dedication as an advisor went beyond simply guiding a graduate student through a thesis; at all times, contained in every conversation and bit of

feedback was his clear intention of support to develop a researcher above anything else. Prof. Vasquez's subject matter knowledge is unquestionable. He is a leader in his field of study, demonstrated by a solid trajectory of study and published research. Nevertheless, Prof. Vasquez has shared with me invaluable experience and guidance not only concerned with the subject matter but also related to professionalism and personal development. His unwavering presence as an advisor shows not only his commitment to the project but to his students as well. Any graduate student would be lucky to have the opportunity to work with Prof. Vasquez. I certainly consider myself lucky to have worked for so long with Prof. Vasquez and even more so to have learned from him what true dedication and commitment to one's work and students in an educational context is. This article would not have been possible without him.

Abstract

Reaction fronts of chemical activity propagate with velocities that depend on the angle of inclination of the container. Buoyancy forces due to changes in chemical composition across the front will affect the velocity and shape of the front. If an external Poiseuille flow is imposed, the conditions of propagation would also change depending on the strength of this flow. Fronts in vertical tubes can change from flat to nonaxisymmetric, and then to axisymmetric as the density gradient is increased. Imposing a Poiseuille flow or tilting the tube changes how this sequence takes place. In this paper, we study the combined effects of convection and forced Poiseuille flow in inclined tubes, solving numerically the reaction-diffusion equations coupled to the Navier-Stokes equations.

Keywords: Nonlinear reaction front, Chemical autocatalysis, Chemical waves, Convection, Advective flows

iv

Contents

List of Figures

1

Chapter 1

Introduction

The interaction of molecular diffusion and an autocatalytic reaction leads to the propagation of fronts of chemical activity [1]. If the propagation takes place in a fluid, fluid motion can alter the speed and shape of the reaction front [2]. Changes in chemical composition across the front may lead to density gradients, which may generate convective flow driven by buoyancy in a gravity field [3, 4, 5]. The concentration gradients can also generate Marangoni flows due to changes in surface tension [6, 7, 8]. Experiments in microgravity studied the effects of fluid flow in chemical reaction fronts due to Marangoni convection [9]. Theoretical work has analyzed the effects of fluid flows in reactions fronts due to compositional changes [10, 11, 12, 13, 14, 15, 16]. In other cases, the fronts propagate in an external fluid velocity field that affects their propagation. Such is the case of fronts in the Belousov-Zhabotinskii reaction propagating in a vortex chain flow [17, 18], or fronts in the iodate-arsenous acid (IAA) reaction propagating in disorder flows [19, 20, 21].

Experiments in the chlorite-thiosulfate reaction inside cylindrical tubes showed that the speed of propagation depends on the angle of inclination, with the speed becoming a maximum at an angle away from the vertical direction [22]. Similar results were found for fronts in the IAA reaction in Hele-Shaw cells [23]. The speed and shape of autocatalytic reaction fronts are modified by imposing a Poiseuille flow [24, 25, 26, 27]. Fronts in the IAA reaction propagating upward in vertical cylindrical tubes showed different speeds and shapes due to convection. As the diameter of the tube is increased, the shape of the fronts change from flat to nonaxisymmetric. Increasing the diameter further results in fronts with an axisymmetric shape [3, 28,

29, 30]. In this work, we will study the combined effects of an imposed Poiseuille flow and gravity driven flow in inclined two-dimensional narrow domains. We will analyze how the advective fluid flow alters the transition between fronts of different symmetry. A previous work showed how the transition to nonaxisymmetric fronts is affected by a Poiseuille flow [31] for vertical propagation. Here we consider an angle of inclination and larger fluid parameters to analyze a second transition in the symmetry of the front. These transitions take place at different parameter values (such as density gradient) if the tube is horizontal, or inclined at a certain angle.

Chapter 2

Equations of motion

The variables describing the system correspond to chemical concentrations of the reacted and unreacted fluids together with the velocity field. We use the Navier-Stokes equations in the Boussinesq approximation to describe fluid motion, therefore the fluid velocity evolves as

$$\frac{\partial \vec{V}}{\partial t} + (\vec{V} \cdot \nabla)\vec{V} = \frac{1}{\rho_0}\nabla P + \nu \nabla^2 \vec{V} + \frac{\rho}{\rho_0}\vec{g}. \tag{2.1}$$

Here P is the pressure, ρ is the mass density of the fluid, ρ_0 is the mass density of the unreacted fluid, ν is the kinematic viscosity, and $\vec{g}$ is the acceleration of gravity. In the Boussinesq approximation, the change of density only modifies the large gravity term, while the continuity equation takes the incompressible form

$$\nabla \cdot \vec{V} = 0. \tag{2.2}$$

A single variable a describes the chemical concentration of the fluid, with $a = a_0$ representing the concentration of the unreacted fluid. As the front propagates, a cubic autocatalytic reaction depletes this concentration, with $a = 0$ becoming the concentration of the reacted fluid. The advection-reaction-diffusion equation

$$\frac{\partial a}{\partial t} + \vec{V} \cdot \nabla a = D\nabla^2 a - k_c a(a_0 - a)^2 \tag{2.3}$$

describes the evolution of the front, where k_c being a rate coefficient, and D

is the coefficient of molecular diffusivity. This equation was applied to fronts observed in experiments in the IAA reaction.

We will solve the equations in a narrow two-dimensional domain resembling a flat tube. The line that runs through the middle of the tube, parallel to its length, will correspond to the z-axis in Cartesian coordinates, with the x-axis perpendicular to it. In an inclined tube, the z-axis makes an angle θ with the vertical direction. The angle $\theta = 0$ corresponds to a vertical tube, therefore in this system of coordinates the acceleration of gravity is written as $\vec{g} = g\sin\theta\hat{x} - g\cos\theta\hat{z}$, where $\hat{x}$ and $\hat{z}$ are unit vectors pointing in the direction of the corresponding axes.

The continuity equation allows us to write the fluid equations in terms of a stream function ψ that provides the components of the velocity $\vec{V}$:

$$V_x = \frac{\partial\psi}{\partial z} \quad , \quad V_z = -\frac{\partial\psi}{\partial x} . \tag{2.4}$$

Taking the curl of the Navier-Stokes equation Eq. (2.1) we arrive to

$$\frac{\partial\omega}{\partial t} = \frac{\partial(\psi,\omega)}{\partial(x,z)} + \nu\nabla^2\omega + \frac{g\cos\theta}{\rho_0}\frac{\partial\rho}{\partial x} + \frac{g\sin\theta}{\rho_0}\frac{\partial\rho}{\partial z} , \tag{2.5}$$

where we defined the vorticity ω as

$$\omega = \nabla^2\psi . \tag{2.6}$$

For two functions f_1 and f_2 we defined

$$\frac{\partial(f_1,f_2)}{\partial(x,z)} = \frac{\partial f_1}{\partial x}\frac{\partial f_2}{\partial z} - \frac{\partial f_1}{\partial z}\frac{\partial f_2}{\partial x} . \tag{2.7}$$

We write the equations of motion in dimensionless form using $t_{ch} = (k_c a_0^2)^{-1}$ as unit of time, $L = (Dt_{ch})^{1/2}$ as unit of length, D as unit of the stream function, D/L^2 as unit of the vorticity, the dimensionless concentration $c = a/a_0$,

$$\frac{\partial\omega}{\partial t} = \frac{\partial(\psi,\omega)}{\partial(x,z)} + \mathrm{S}_c\nabla^2\omega + \mathrm{RaS}_c\left(\cos\theta\frac{\partial c}{\partial x} + \sin\theta\frac{\partial c}{\partial z}\right) \tag{2.8}$$

and

$$\frac{\partial c}{\partial t} = \frac{\partial(\psi,c)}{\partial(x,z)} + \nabla^2 c - c(1-c)^2 . \tag{2.9}$$

5

We defined a dimensionless Rayleigh number

$$\text{Ra} = \frac{g\delta L^3}{\nu D} \tag{2.10}$$

and a dimensionless Schmidt number

$$S_c = \frac{\nu}{D} \ . \tag{2.11}$$

The parameter δ represents the fractional density difference between the unreacted fluid and the reacted fluid. We assumed that the density varies linearly with the concentration c. For fronts in the IAA reaction, the Schmidt number is large, we will use Eq. (2.8) in the limit of infinite Schmidt number [16]

$$\nabla^2 \omega + \text{Ra} \left(\cos\theta \frac{\partial c}{\partial x} + \sin\theta \frac{\partial c}{\partial z} \right) = 0 \ . \tag{2.12}$$

We study the effects of a Poiseuille flow imposed on a reaction front combined with gravity driven convection. To this end we write the fluid velocity as $\vec{V} = \vec{V}_p + \vec{V}'$. Here the Poiseuille flow corresponds to $\vec{V}_p(x, z) = 6\bar{V}x(a-x)/a^2\hat{z}$, with $\bar{V}$ being the average speed. We can use a stream function representing the Poiseuille flow velocity, and another representing the remaining flow $\vec{V}'$, then substitute the total stream function into Eq. (2.12), which is linear. This results in an identical equation, applied only to the flow $\vec{V}'$ [31]. With these changes, we solve Eq. (2.12) to obtain the portion of the flow driven by gravity and then adding the Poiseuille flow to find the total flow in Eq. (2.8).

Chapter 3

Numerical Methods

The time evolution of the system is defined by the advection-reaction-diffusion [Eq. (2.9)], coupled to the Stokes equation [Eq. (2.10)]. We use a finite difference method on a $N_x \times N_z$ rectangular mesh to approximate the spatial derivatives of all variables, while finite differences in time provide the values after a time step Δt following a simple Euler method. The discrete set of variables c_{ij}^h corresponds to the value of the concentration c at the mesh point at x_i, z_j for the discrete time t_h. We obtain the values at the boundaries from the no flow boundary conditions for c. Using the Euler method on Eq. (2.9), we obtain evolution for the concentrations at the time t_{h+1} from the known values of the variables at time t_h.

$$
\begin{aligned}
c_{i,j}^{h+1} = c_{i,j}^h + \Delta t \Bigg[& \frac{(\psi_{i+1,j}^h - \psi_{i-1,j}^h)(c_{i,j+1}^h - c_{i,j-1}^h)}{4\Delta x \Delta z} \\
& - \frac{(c_{i+1,j}^h - c_{i-1,j}^h)(\psi_{i,j+1}^h - \psi_{i,j-1}^h)}{4\Delta x \Delta z} + \frac{c_{i+1,j}^h - 2c_{i,j}^h + c_{i-1,j}^h}{(\Delta x)^2} \\
& + \frac{c_{i,j+1}^h - 2c_{i,j}^h + c_{i,j-1}^h}{(\Delta z)^2} - c_{i,j}^h(1 - c_{i,j}^h)^2 - V_z^p \frac{c_{i,j+1}^h - c_{i,j-1}^h}{2\Delta z} \Bigg] .
\end{aligned} \tag{3.1}
$$

Once we obtain the values of the concentration at the time step t_{h+1}, we proceed to solve for the vorticity and stream function at that time step. Replacing the vorticity from Eq. (2.5) into Eq. (2.8), we arrive into a double-Poisson equation for the stream function.

$$\nabla^2 \nabla^2 \psi = -\text{Ra} \left(\cos \theta \frac{\partial c}{\partial x} + \sin \theta \frac{\partial c}{\partial z} \right) \equiv F(x, z) . \qquad (3.2)$$

This equation indicates that the stream function is fully determined at one instant by the values of the concentration c, leading to the function F through its derivatives. The function F is zero away from the front since the concentration c is constant in that region. Therefore we can introduce in Eq. (3.2) a couple of Fourier sine series along the z direction:

$$\psi(x, z) = \sum_n \psi_n(x) \sin(k_n z) \qquad (3.3)$$

$$F(x, z) = \sum_n F_n(x) \sin(k_n z) , \qquad (3.4)$$

Making the coefficients of each sine function equal to each other in both sides of the equation, we find a set of N_z independent ordinary differential equations for each index n

$$\frac{d^4 \psi_n}{dx^4} - 2k_n^2 \frac{d^2 \psi_n}{dx^2} + k_n^4 = F_n(x) . \qquad (3.5)$$

To solve this set of equations, we first need to compute the functions $F_n(x)$ using an orthogonal projection of $F(x, z)$ over the corresponding sine functions. Since the values of the concentration c are given on a rectangular mesh, we can only obtain F_n at the coordinates x_i. The orthogonal projection over the sine functions is carried out using a discrete fast Fourier algorithm with function $F(x_i, z_j)$ using the points on the mesh [37]. Given that there is N_z discrete points in the z direction, we will have n=1,2,....N_z different coefficients F_n.

Each equation in Eqs. (3.5) has the form

$$\frac{d^4 \phi}{dx^4} - 2k^2 \frac{d^2 \phi}{dx^2} + k^4 = \tilde{F}(x) . \qquad (3.6)$$

In this equation, we apply finite difference approximations for the derivatives using the mesh points in the x direction. This results in a set of $N_x - 4$ independent finite difference equation on the index m

$$\frac{\phi_{m-2} - 4\phi_{m-1} + 6\phi_m - 4\phi_{m+1} + \phi_{m+2}}{(\Delta x)^4}$$
$$- 2k^2 \frac{\phi_{m-1} - 2\phi_m + \phi_{m+1}}{(\Delta x)^2} + k^4 \phi_m = \tilde{F}_m \; ,$$
$$\text{with } m = 3, ... N_x - 2. \quad (3.7)$$

The boundary conditions at the walls provide the values of ϕ near the boundaries. Since the stream function vanishes at the walls we have $\phi_1 = \phi_{N_x} = 0$. The normal derivative of the stream function vanishes which allow us to determine further conditions. Using a Taylor expansion up to order $(\Delta x)^2$ in the left wall, we have

$$\phi_2 = \phi_1 + \frac{d\phi_1}{dx}(\Delta x) + \frac{1}{2}\frac{d^2\phi_1}{dx^2}(\Delta x)^2 + o(\Delta x^3) \; . \quad (3.8)$$

This is simplified given that the stream function and its derivative vanish at the wall, corresponding to $\phi = d\phi/dx = 0$. The second derivative at wall can be replaced with the second derivative at next point to the right (i=2) while keeping the same order of the approximation. After using the finite difference expression for this second derivative, we arrive to the condition $\phi_2 = \phi_3/4$. Each equation from the set Eq. (3.7) involves the four nearest neighbors to a location m. Consequently, each equation can be written as

$$\gamma\phi_{m-2} - \beta\phi_{m-1} + \alpha\phi_m - \beta\phi_{m+1} + \gamma\phi_{m+2} = \tilde{F} \quad (3.9)$$

with

$$\alpha = \frac{6}{(\Delta x)^4} + \frac{4k^2}{(\Delta x)^2} + k^4 \quad (3.10)$$

$$\beta = \frac{4}{(\Delta x)^4} + \frac{2k^2}{(\Delta x)^2} \quad (3.11)$$

$$\gamma = \frac{1}{(\Delta x)^4} \; . \quad (3.12)$$

The previous linear system of equations can be written in terms of the corresponding coefficients using a pentadiagonal matrix

$$
\begin{pmatrix}
b_1 & c_1 & f_1 & 0 & 0 & . & & & & \\
a_2 & b_2 & c_2 & f_2 & 0 & . & & & & \\
e_3 & a_3 & b_3 & c_3 & f_3 & . & & & & \\
0 & e_4 & a_4 & . & . & & . & & & \\
0 & 0 & . & . & . & & . & & . & \\
& & e_i & a_i & b_i & & c_i & & f_i & \\
& & & . & . & . & & . & & . \\
& & & & e_{N-1} & a_{N-1} & b_{N-1} & c_{N-1} \\
& & & & & e_N & a_N & b_N
\end{pmatrix}
\cdot
\begin{pmatrix}
g_1 \\ g_2 \\ g_3 \\ . \\ . \\ . \\ . \\ g_{N-1} \\ g_N
\end{pmatrix}
=
\begin{pmatrix}
d_1 \\ d_2 \\ d_3 \\ . \\ . \\ . \\ . \\ d_{N-1} \\ d_N
\end{pmatrix}
\tag{3.13}
$$

with

$$
b_1 = b_N = \alpha - \frac{\beta}{4}
$$
$$
a_2 = c_{N-1} = \frac{\gamma}{4} - \beta \ .
$$

The remaining constants for all other indices are

$$
b_i = \alpha \ ,
$$
$$
a_i = c_i = -\beta \ ,
$$
$$
e_i = f_i = \gamma \ .
\tag{3.14}
$$

In the system of equations in matrix form defined by Eq. (3.13), the unknowns correspond to $g_i = \phi_{i+2}$, and the equations are equal to $d_i = \tilde{F}_{i+2}$. The system can be solved using a modified Thomas algorithm, which provides the results after two forward and backward sweeps [32].

10

Chapter 4

Results

4.1 Vertical tube

We set a propagating front in a two-dimensional vertical tube using an initial concentration of unreacted fluid ($c = 1$) in the upper half of the tube, a concentration of reacted fluid ($c = 0$) in the lower half, adding small random perturbations near the interface. The evolution results in a moving interface separating fluids of different densities. For tubes of small width, the front becomes flat without convection even if the less dense fluid is underneath. This solution corresponds to the analytical solution of the one-dimensional reaction-diffusion equation [34] showing a dimensionless speed equal to $1/\sqrt{2}$. The analytical result assumes an infinite domain where the front can travel. Since our computational domain is finite, we shift the front backward after it travels a short distance, adding unreacted fluid far away from the front. In this manner, we can study the front propagation indefinitely. Increasing the Rayleigh number results in a transition to convection as the flat front looses stability to buoyancy [36]. Near the transition to convection the front takes a steady non-axisymmetric shape that propagates with a constant speed higher than the flat front speed [35]. The shape of the front is determined by a single convective roll propagating with the front as shown in Fig. 4.1a. Increasing the Rayleigh number further , we found a new axisymmetric state that consists of two convective rolls as shown in Fig. 4.1b. In this case, fluid rises through the center of the tube and falls along the walls determining the shape of the front. We will study the effects of an external Poiseuille flow imposed on these states.
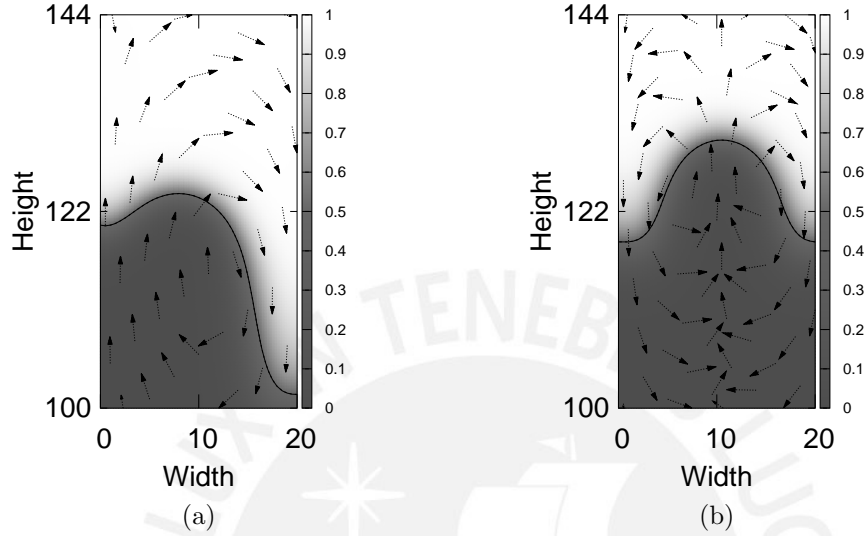
Figure 4.1: Chemical concentrations in reaction fronts with convection. The arrows indicate the direction of fluid motion. In the nonaxisymmetric front (a) the fluid rises in one side of the tube and falls in the opposite side. For the axisymmetric front (b) the fluid rises near the center and falls along both sides.

We calculate the speed of the front as a function of Rayleigh number for different values of the average speed of a Poiseuille flow $\bar{V}$. Near the transition to convection (without Poiseuille flow) the front speed increases as we increase the Rayleigh number, as shown in Fig. 4.2. The front velocity keeps increasing with larger Rayleigh numbers until it reaches a maximum. The shape of the front remains non-axisymmetric until it reaches an Ra value where the speed decreases abruptly. At this point, the front takes an axisymmetric shape. The type of convection also determines the front speed, since near the transition we can have higher speeds for non-axisymmetric fronts, even if the Rayleigh numbers are smaller. In the case of axisymmetric fronts, larger values of the Rayleigh number lead to higher front velocities.

The addition of an advective Poiseuille flow modifies the shape and the speed of convective reaction fronts. We first consider a supportive flow moving in the same direction as the front without Poiseuille flow. In our case we set this front to propagate in the positive z direction, with the average
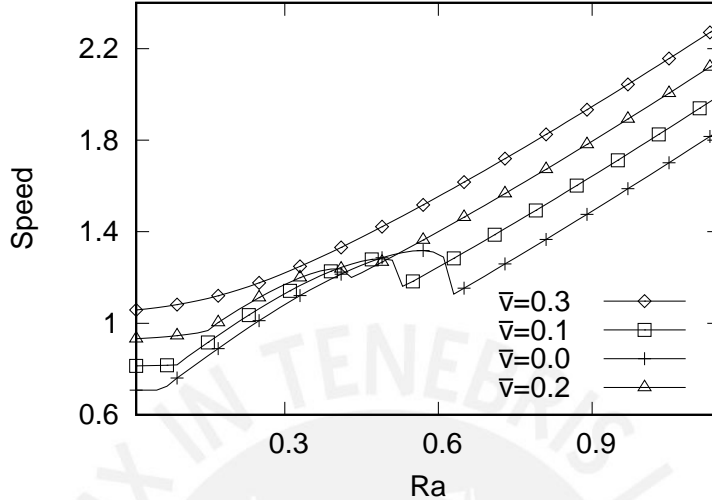
12

Figure 4.2: The dimensionless front speed as a function of the Rayleigh number for different values of the Poiseuille flow. The + signs correspond to $\bar{V}$=0.0, the squares correspond to $\bar{V}$=0.1, the triangles correspond to $\bar{V}$=0.2 and the rhombuses correspond to $\bar{V}$=0.3.

velocity of the Poiseuille flow positive. Flat fronts in narrow tubes acquire a slight axisymmetric shape caused by the parabolic profile of the Poiseuille flow. In these cases, gravity driven convection sets in due to a horizontal density gradient. The advective Poiseuille flow plus convection enhances the speed as shown in Fig. 4.2. Near Ra=0, the fronts with a Pouiseuille flow increase slightly their speed as a function of the Rayleigh number, whereas without the flow all flat fronts have the same constant speed. If the flow is not too strong, we still observe a transition to a nonaxisymmetric front, however it takes place at higher values of the Rayleigh number. This speed reaches a maximum and decreases while the front remains nonaxisymmetric. The subsequent transition to axisymmetric fronts now occurs at a smaller value of Ra, thus narrowing the range where nonaxisymmetric fronts can appear.

This range disappears completely for a Poiseuille flow with $\bar{V}$=0.2. In this case there is no transition to a nonaxisymmetric front regardless of the Rayleigh number. Nonaxisymmetric fronts with a supportive flow can occur only for small $\bar{V}$ on a narrower range of Rayleigh numbers.
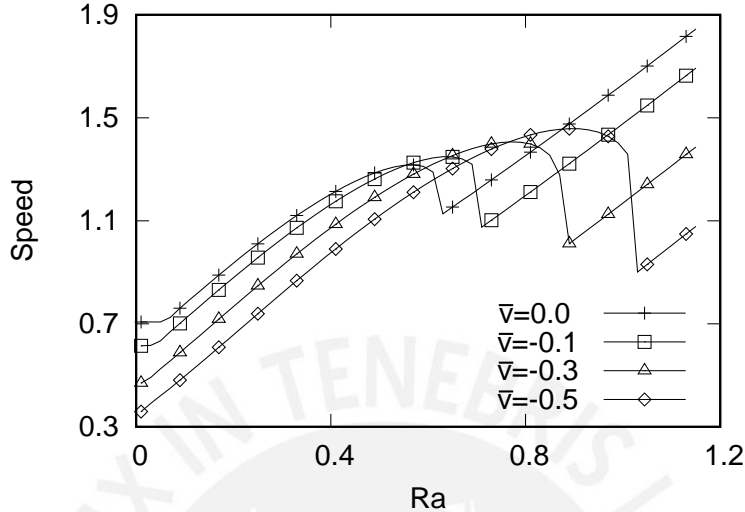
13

Figure 4.3: The dimensionless front speed as a function of the Rayleigh number for different negative average velocities of the Poiseuille flow. The results correspond to the reaction-diffusion-convection equation. The + signs correspond to $\bar{V}$=0.0, the squares correspond to $\bar{V}$=-0.1, the triangles correspond to $\bar{V}$=-0.3 and the rhombuses correspond to $\bar{V}$=-0.5.

In the case of adverse Poiseuille flows in the opposite direction ($\bar{V} <$ 0), we find that nonaxisymmetric fronts always take place for the velocities studied ($\bar{V} \geq$ -0.5). For Rayleigh numbers near zero the front is almost flat, but increasing $\bar{V}$ in the negative direction results in nonaxisymmetric fronts [Fig. 4.3]. In the case of $\bar{V}$=-0.1, we find a transition from the near flat front to a nonaxisymmetric front as we increase the Rayleigh number. In contrast, for $\bar{V}$=-0.2 and -0.3, the initial front is already nonaxisymmetric, increasing its speed as we increase Ra. As the Rayleigh number is increased further, a transition to an axisymmetric front takes place where the front speed decreases abruptly [Fig. 4.3]. We find that the transition takes place at larger Rayleigh numbers for stronger flows in the opposite direction. In these cases, the net result of using an adverse axisymmetric Poiseuille flow is to strengthen the nonaxisymmetric state.

The front speed changes with the average velocity of the Poiseuille flow, however it does not always increases with supportive flows, nor decreases with adverse flows. In the case of Rayleigh numbers close to the transition
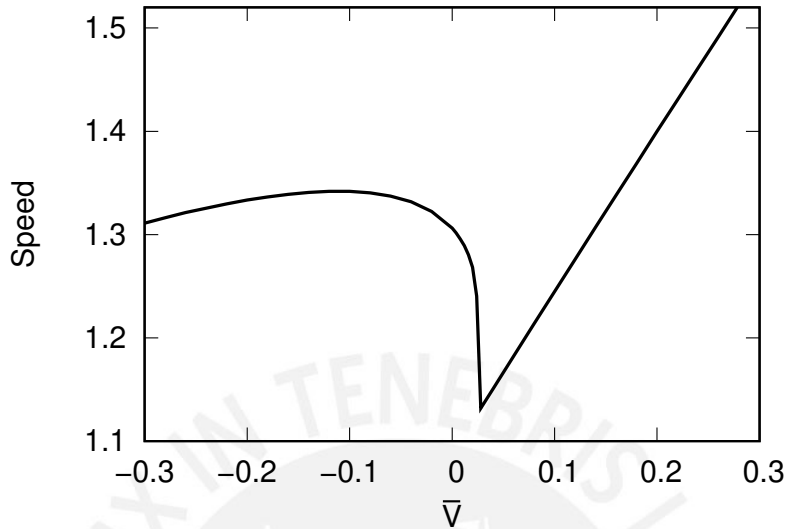
14

Figure 4.4: The front speed as a function of $\bar{V}$, the average velocity of the Poiseuille flow. At $\bar{V} = 0$ the front is nonaxisymmetric (Ra=0.6). A small supportive speed ($\bar{V} > 0$) diminishes the front speed, while a small adverse speed ($\bar{V} < 0$) increases the front speed. At larger values of the flow speed, the change of velocity follows the direction of $\bar{V}$.

to axisymmetric fronts, we find that the change of speed is opposite to the direction of the Poiseuille flow. In Fig. 4.4 we display the speed of the front as a function of the average flow speed ($\bar{V}$) keeping the Rayleigh number constant (Ra=0.6). For $\bar{V}=0$, the front is a convective axisymmetric front traveling faster than convectionless flat fronts. As we introduce a supportive flow, increasing $\bar{V}$ leads to a decrease in the front velocity. Consequently, as we push the front in the same direction, the front slows down. This behavior takes place until $\bar{V}=0.028$, where the front begins to increase its speed monotonically. At that point, the front changes from non-axisymmetric to axisymmetric. On the other hand, if we start to push against the initial front, we observe that the front speed increases until it reaches a maximum value near $\bar{V}=-0.11$, it then decreases as the strength of the adverse flow increases. This behavior takes place for Rayleigh numbers close to the transition between convective fronts.
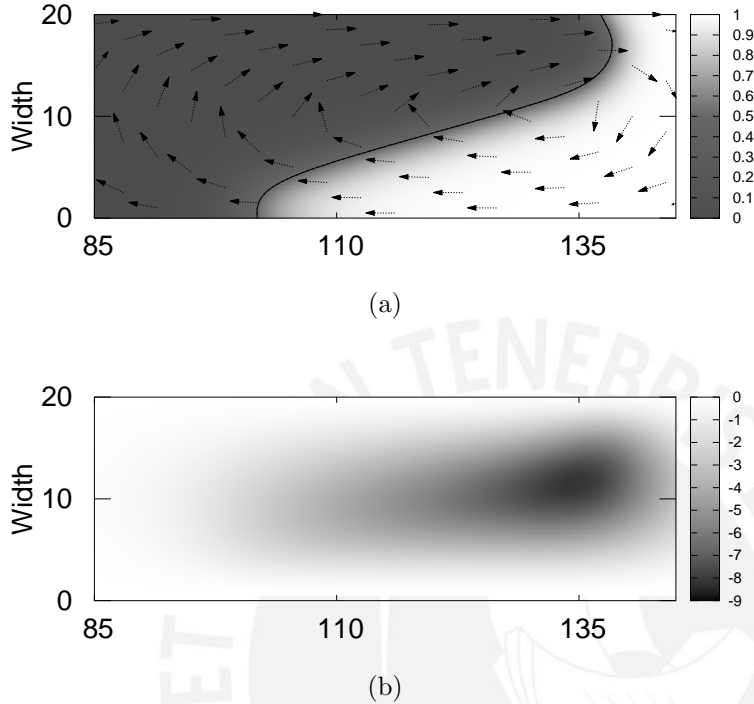
(a)

(b)

Figure 4.5: Representation of the chemical concentration (top) and stream function (bottom) for $Ra = 0.65$ in a horizontal tube.

4.2   Horizontal tube

Fronts in horizontal tubes generate horizontal concentration gradients, consequently convection will always be present as long as the Rayleigh number is nonzero. In Fig. 4.5 we show a nonaxisymmetric reaction front due to single convective roll. The shape remains steady as it travels along the tube with constant speed. We notice that near the interface the less dense reacted fluid is above the unreacted fluid due to buoyancy, as expected. This speed is higher than the reaction-diffusion front due to convection. Increasing the Rayleigh number increases the strength of the convective flow, resulting in higher front speeds (Fig. 4.6). As we introduce a supportive Poiseuille flow, the speed of the front increases, maintaining a nonaxisymmetric shape (Fig. 4.6). For adverse Poiseuille flows, we still observe a nonaxisymmetric front, but the speed of the front decreases. In vertical tubes near a symmetry transition, we find situations where the speed increases for adverse Poiseuille

flows. This transition does not take place in horizontal tubes, having the speed of the front decreasing with adverse flows.
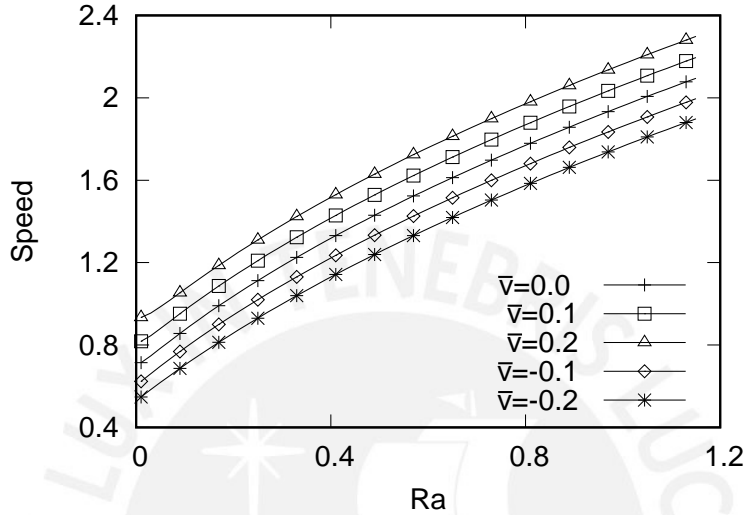

Figure 4.6: The dimensionless front speed as a function of the Rayleigh number for different average velocities of the Poiseuille flow. The tube is completely horizontal. The crosses correspond to $\bar{V}$=0.0, the squares correspond to $\bar{V}$=0.1, the triangles correspond to $\bar{V}$=0.2, the rhombuses correspond to $\bar{V}$=-0.1 and the asterisks correspond to $\bar{V}$=-0.2.

4.3 Inclined tube

The front shape and speed change as we tilt the tube away from the vertical direction. We show in Fig. 4.7 the change of speed as a function of tilt angle when the Rayleigh number is Ra=0.4. In this figure, we compare the effect of the angle for fronts traveling under different Poiseuille flows. For vertical tubes, these fronts are nonaxisymmetric fronts, with their velocity varied in the same direction of the applied flow: a supportive flow increases the speed, while an adverse flow reduces it. As we tilt the tube, the front speed increases, reaching a maximum value of 43.2 degrees, before it starts to decrease. This result is consistent with previous studies at different conditions showing maximum speed for angles away from the vertical direction [22]. This effect is related to the Boycott effect observed in sedimentation,
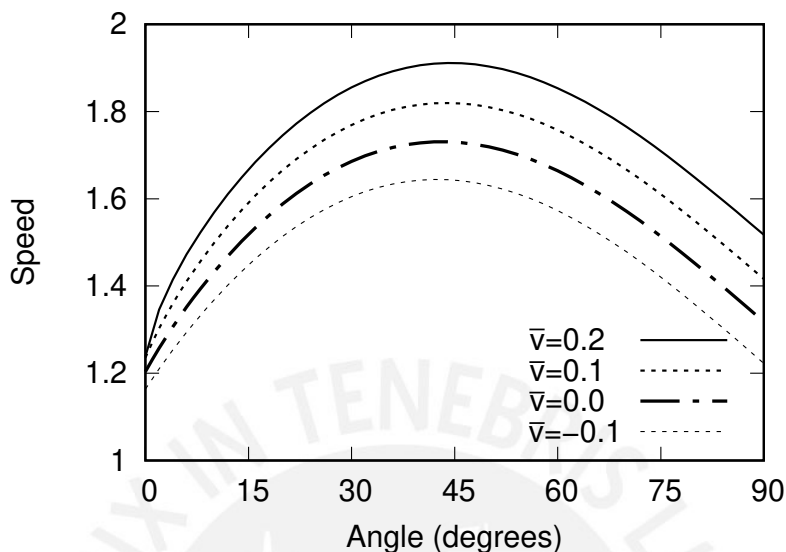
17

Figure 4.7: The front speed as a function of the angle from the vertical direction in the presence of Poiseuille flow. The front in the vertical direction is nonaxisymmetric with Ra=0.4. Fronts are initiated from a flat chemical interface with small random perturbations.

where the process takes place more rapidly in an inclined tube [33]. We still find a similar behavior for fronts with a Poiseuille flow. The angle for maximum speed changes with the flow, for $\bar{V}$=-0.1 it is 42.5 degrees, compared to 44.5 degrees for $\bar{V}$=0.2, showing the influence of supportive flow. As we move from vertical to horizontal tubes, the change in front velocities is larger for the same Poiseuille flow. In Fig. 4.7, we notice that the front speeds are more spread apart in the horizontal than in the vertical direction, thus the effect of the external flow is larger if the tube is horizontal. Gravity plays a more important role in the vertical propagation since the velocities are closer to each other for different external flows. For a higher Rayleigh number (Ra=0.8), the shape of fronts in the vertical direction exhibit a maximum away from the walls, a consequence of two convective rolls. The external Poiseuille flow changes the velocities in the vertical direction, however as the tube is tilted, the front velocities become closer for the different flows. In Fig. 4.8, we observe that in each curve, the speed increases as we increase the angle, but each curve presents an inflection point. The front speed reaches a maximum, as in the previous case, and then decreases as the front becomes
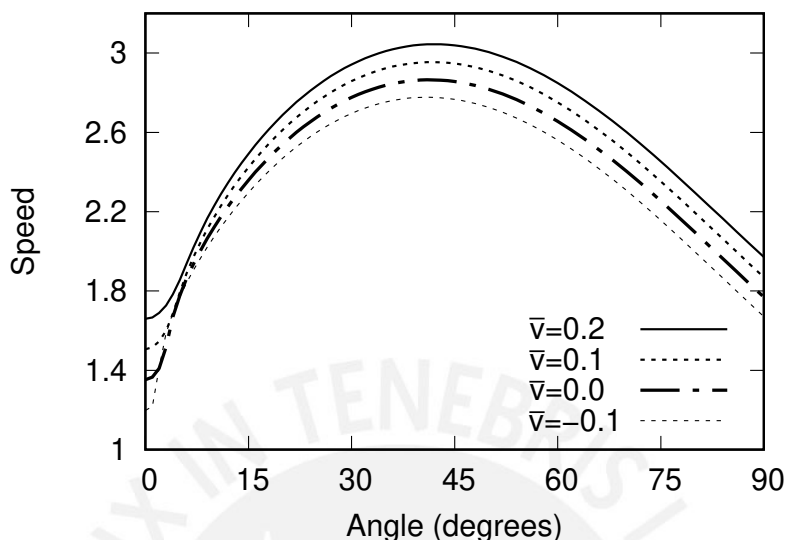
Figure 4.8: The front speed as a function of the angle from the vertical direction in the presence of Poiseuille flow. The front in the vertical direction is axisymmetric with Ra=0.8. Fronts are initiated from a flat chemical interface with small random perturbations.

horizontal. The reason for the inflection point is because a front in vertical tubes without an external flow is axisymmetric, while in an horizontal tube is non-axisymmetric. In the previous case (Ra=0.4), the front was nonaxisymmetric even in vertical tubes. The angle for maximum speed corresponds to 41.4 degrees for fronts without external flows. Fronts in a Poiseuille flow also exhibit a maximum speed, but the angle changes slightly with the flow. It corresponds to 41 degrees for an adverse flow with $\bar{V}$=-0.1, and 42.2 degrees for a supportive flow with $\bar{V}$=0.2. As in the previous case, the maximum speed takes place at larger angles for higher supportive flows.

In the case of Ra=0.4, we have a non-axisymmetric front propagating upward in a vertical tube. In this case, there are two identical mirror-like solutions, however as we tilt the tube, we find that these solutions separate acquiring different speeds. Fig. 4.9 shows a region of bistability between both solutions, one solution increases its speed with tilting angle, while the other decreases. Eventually, the front with lower solution looses stability, while the other remains stable. Applying a Poiseuille flow in these tubes allows a larger region of bistability if the flow is adverse to the direction of

19

propagation, while it reduces the region of bistability in the other front.
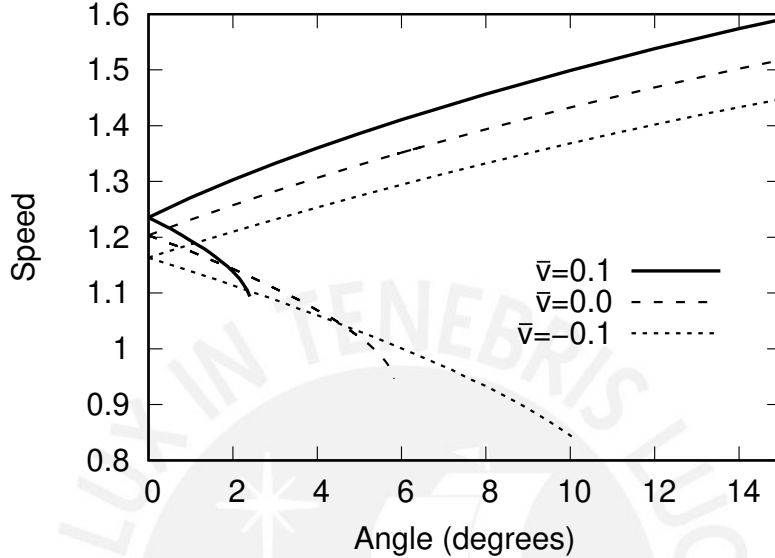

Figure 4.9: The speed of the front as a function of tilt angle. The system allows two mirror nonaxisymmetric states with the same velocity (Ra=0.4). As the tube is tilted, they adquire different speeds for small angles. Larger angles allow only one state.

We investigate the front speed as function of Rayleigh number for fixed Poiseuille flows in inclined tubes. In Fig. 4.10 we show the speed for steady fronts initiated from a flat interface with small random perturbations. Without an external flow (Fig. 4.10b), the front velocity increases as the Rayleigh number increases, reaching a maximum near the transition from axisymmetric to non-axisymmetric fronts. After the transition, the front increases its velocity once again. The same behavior is observed for slightly inclined tubes, but with higher speeds at each Rayleigh number. We also notice that the previous transition between fronts is smoothed, since in tilted tubes all fronts have a non-axisymmetric component. The local minimum near the transition gets shifted to the right. At larger Rayleigh numbers, the dependence between the speed and the Rayleigh number is almost linear. Imposing a Poiseuille flow changes the speed dependence with Ra according to whether the flow is supportive or adverse to the front. The local minimum in each curve takes place at a lower value of Ra for supportive flows, where the opposite is true in adverse flows. For values of Ra near zero, and values beyond

the transition, the front speed is larger for the supportive flow. Near the transition it is not always the case, due to the shift of the local minimum.

(a) $\bar{V} = 0.1$

(b) $\bar{V} = 0.0$

(c) $\bar{V} = -0.1$

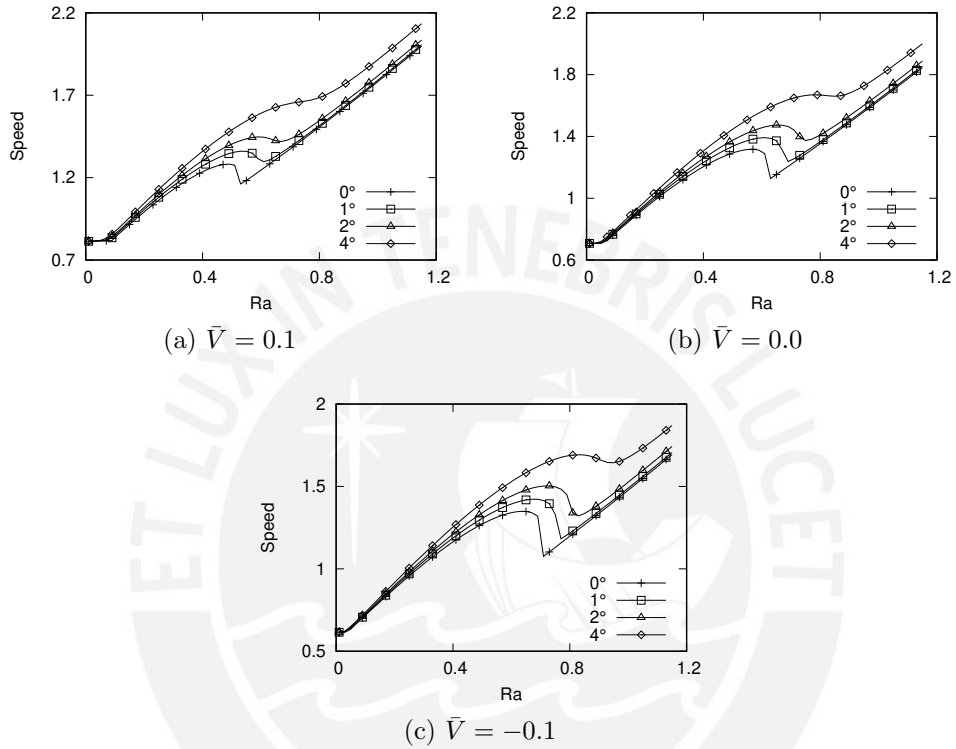Figure 4.10: The speed of the front as a function of the Rayleigh number for different tilt positions of the two dimensional tube. The crosses correspond to a vertical position of the tube, the squares correspond to a 1 degree tilt from the vertical position, the triangles correspond to a 2 degree tilt from the vertical position and the rhombuses correspond to a 4 degree tilt from the vertical position.

Chapter 5

Conclusions

In this paper we studied the effects of fluid flow in the propagation of auto-catalytic reaction fronts. We analyzed the effects of convective fluid motion in a two-dimensional domain using a fast Fourier algorithm and a modified Thomas method to solve a pentadiagonal matrix along the width of the domain. The fluid motion is caused by a change in density across the front, with an imposed Poiseuille flow in a two dimensional tube. The convective flow can take place in horizontal tubes and vertical tubes. Adding an external Poiseuille flow will always result in a curved front, therefore convection will be present due to the horizontal density gradients. Without an external flow, the front changes from flat to nonaxisymmetric in a vertical tube, as the Rayleigh number is increased. In either case the initial flat front is curved by the flow, with the transition to a nonaxisymmetric front modified depending on the direction of propagation of the flow. Supportive Poiseuille flows will move the transition to higher Rayleigh numbers, while strong enough adverse flows will make the transition disappear.

We also analyzed the effects in convective fronts as we tilt the tube. We found that the speed of propagation becomes higher as we tilt the tube away from the vertical direction, reaching a maximum at a certain angle, then decreasing as the tube becomes horizontal. The angle for maximum speed depends on the Rayleigh number and the strength of the Poiseuille flow. Tilting the angle also results in a region of bistability for nonaxisymmetric fronts. In this case the fronts are higher on one side of the tube, then tilting towards or away from the elevation will lead to different states. However, for larger tilting angles only one state is present. The application of Poiseuille flow in convective reaction fronts can be tested in experiments, however careful con-

sideration has to be placed when comparing the two dimensional results with experiments either cylindrical tubes or confined Hele-Shaw cells. Further calculations in three dimension are necessary to provide a complete account of these cases.

Data availability statement Data generated and/or analyzed during the current study are available from corresponding authors upon reasonable request.

Bibliography

[1] Epstein, I.R., Pojman J.A.: An introduction to nonlinear chemical dynamics: oscillations, waves, patterns, and chaos. Oxford university press, Oxford (1998).

[2] Miike, H., Müller, S.C., Hess, B.: Hydrodynamic flows traveling with chemical waves. Phys. Lett. A (1989).

[3] Pojman, J. A., Epstein, I. R., McManus, T. J., Showalter, K.: Convective effects on chemical waves. 2. Simple convection in the iodate-arsenous acid system. The Journal of Physical Chemistry, **95**(3), 1299-1306 (1991).

[4] Pojman, J. A., Nagy, I.P., Epstein, I.R.: Convective effects on chemical waves. 3. Multicomponent convection in the iron (II)-nitric acid system. The Journal of Physical Chemistry **95**(3), 1306-1311 (1991).

[5] Böckmann, M., Müller, S.C.: Growth rates of the buoyancy-driven instability of an autocatalytic reaction front in a narrow cell. Phys. Rev. Lett. **85**(12), 2506 (2000).

[6] Eckert, K., Acker, M., Tadmouri, R., Pimienta, V.: Chemo-Marangoni convection driven by an interfacial reaction: Pattern formation and kinetics. Chaos: An Interdisciplinary Journal of Nonlinear Science, **22**(3), 037112 (2012).

[7] Hauser, M.J.B, Simoyi, R.H.: Inhomogeneous precipitation patterns in a chemical wave. Effect of thermocapillary convection. Chem. Phys. Lett. **227**(6), 593-600 (1994).

[8] Horváth, D., Budroni, M. A., Bába, P., Rongy, L., De Wit, A., Eckert, K., Hauser, M.J.B, Tóth, Á.: Convective dynamics of traveling autocatalytic

fronts in a modulated gravity field. Phys. Chem. Chem. Phys. **16**(47), 26279-26287 (2014).

[9] Bába, P., Rongy, L., De Wit, A., Hauser, M. J. B., Tóth, Á., Horváth, D.: Interaction of pure Marangoni convection with a propagating reactive interface under microgravity. Phys. Rev. Lett. **121**(2), 024501 (2018).

[10] De Wit, A.: Fingering of chemical fronts in porous media. Phys. Rev. Lett. **87**(5), 054502 (2001).

[11] Jotkar, M., Rongy, L., De Wit, A.: Chemically-driven convective dissolution. Phys. Chem. Chem. Phys. **21**(35), 19054-19064 (2019).

[12] Jotkar, M., Rongy, L., De Wit, A.: Reactive convective dissolution with differential diffusivities: Nonlinear simulations of onset times and asymptotic fluxes. Phys. Rev. Fluids **5**(10), 104502 (2020).

[13] D'Hernoncourt, J., Merkin, J.H., De Wit, A.: Interaction between buoyancy and diffusion-driven instabilities of propagating autocatalytic reaction fronts. I. Linear stability analysis. J. Chem. Phys. **130**(11), 114602 (2009)

[14] D'Hernoncourt, J., Merkin, J.H., De Wit, A.: Interaction between buoyancy and diffusion-driven instabilities of propagating autocatalytic reaction fronts. II. Nonlinear simulations. J. Chem. Phys. **130**(11), 114503 (2009)

[15] Vasquez, D. A., Littley, J. M., Wilder, J. W., Edwards, B. F.: Convection in chemical waves. Physical Review E, **50**(1), 280-284 (1994).

[16] Vasquez, D.A., Thoreson, E.: Convection in chemical fronts with quadratic and cubic autocatalysis. Chaos **12**(1), 49-55 (2002).

[17] Mahoney, J. R., Li, J., Boyer, C., Solomon, T., Mitchell, K. A.: Frozen reaction fronts in steady flows: A burning-invariant-manifold perspective. Physical Review E, **92**(6), 063005 (2015).

[18] Schwartz, M. E., and T. H. Solomon.: Chemical reaction fronts in ordered and disordered cellular flows with opposing winds. Phys. Rev. Lett. **100**(2), 028302 (2008).

[19] Chevalier, T., Salin, D., Talon, L.: Frozen fronts selection in flow against self-sustained chemical waves. Phys. Rev. Fluids **2**(4), 043302 (2017).

[20] Atis, S., Saha, S., Auradou, H., Salin, D., Talon, L.: Autocatalytic reaction fronts inside a porous medium of glass spheres. Physical review letters **110**(14), 148301 (2013).

[21] Gueudré T., Dubey, A. K., Talon, L., Rosso, A.: Strong pinning of propagation fronts in adverse flow. Phys. Rev. E **89**(4), 041004 (2014).

[22] Nagypal, I.,Bazsa, G., Epstein, I. R.: Gravity-induced anisotropies in chemical waves. Journal of the American Chemical Society **108**(13), 3635-3640 (1986).

[23] Jarrige, N., Malham, I. B., Martin, J., Rakotomalala, N., Salin, D., Talon, L.: Numerical simulations of a buoyant autocatalytic reaction front in tilted Hele-Shaw cells. Phys. Rev. E **8**1(6), 066311 (2010).

[24] Edwards, B. F.: Poiseuille advection of chemical reaction fronts. Phys. Rev. Lett. **89**(10), 104501 (2002).

[25] Spangler, R. S., Edwards, B. F.: Poiseuille advection of chemical reaction fronts: Eikonal approximation. The Journal of chemical physics **118**(13), 5911-5915 (2003).

[26] Leconte, M., Martin, J., Rakotomalala, N., Salin, D.: Pattern of reaction diffusion fronts in laminar flows. Phys. Rev. Lett. **90**(12), 128302 (2003).

[27] Leconte, M., Martin, J., Rakotomalala, N., Salin, D., Yortsos, Y. C.: Mixing and reaction fronts in laminar flows. The Journal of chemical physics **120**(16), 7314-7321 (2004).

[28] Masere, J., Vasquez, D. A., Edwards, B. F., Wilder, J. W., Showalter, K.: Nonaxisymmetric and axisymmetric convection in propagating reaction-diffusion fronts. The Journal of Physical Chemistry **98**(26), 6505-6508 (1994).

[29] Vasquez, D. A., Edwards, B. F., Wilder, J. W.: Onset of convection for autocatalytic reaction fronts: Laterally bounded systems. Phys Rev A **43**(12), 6694 (1991).

[30] Vasquez, D. A., Wilder, J. W., Edwards, B. F.: Convective instability of autocatalytic reaction fronts in vertical cylinders. Physics of Fluids A: Fluid Dynamics **4**(11), 2410-2414 (1992).

[31] Vasquez, D. A.:Convective chemical fronts in a Poiseuille flow. Phys. Rev. E **76**(5), 056308 (2007).

[32] Fletcher, C. A. J.: Computational Techniques for Fluid Dyanmmics, Springer-Verlag, Berlin (1991).

[33] Boycott, A. E.: Sedimentation of blood corpuscles. Nature **104**, 532 (1920)

[34] Showalter, K.: Quadratic and cubic reaction-diffusion fronts. Nonlinear Science Today **4**(4), 1-2 (1994).

[35] Vasquez, D. A., Coroian, D. I.: Stability of convective patterns in reaction fronts: A comparison of three models. Chaos: An Interdisciplinary Journal of Nonlinear Science **20**(3), 033109 (2010).

[36] Vasquez, D. A., Wilder, J. W., Edwards, B.F.: Hydrodynamic instability of chemical waves. The Journal of chemical physics **98**(3), 2138-2143 (1993).

[37] Press, W.H., Teukolsky, S.A., Vetterling, W.T, Flannery, B.P.: Numerical Recipes: The Art of Scientific Computing Third Edition. Cambridge university press, Cambridge (2011).